Dynamics of submarine debris flow and tsunami

Shiva P. Pudasaini

Acta Mechanica

ISSN 0001-5970
Volume 225
Number 8

Acta Mech (2014) 225:2423-2434
DOI 10.1007/s00707-014-1126-0

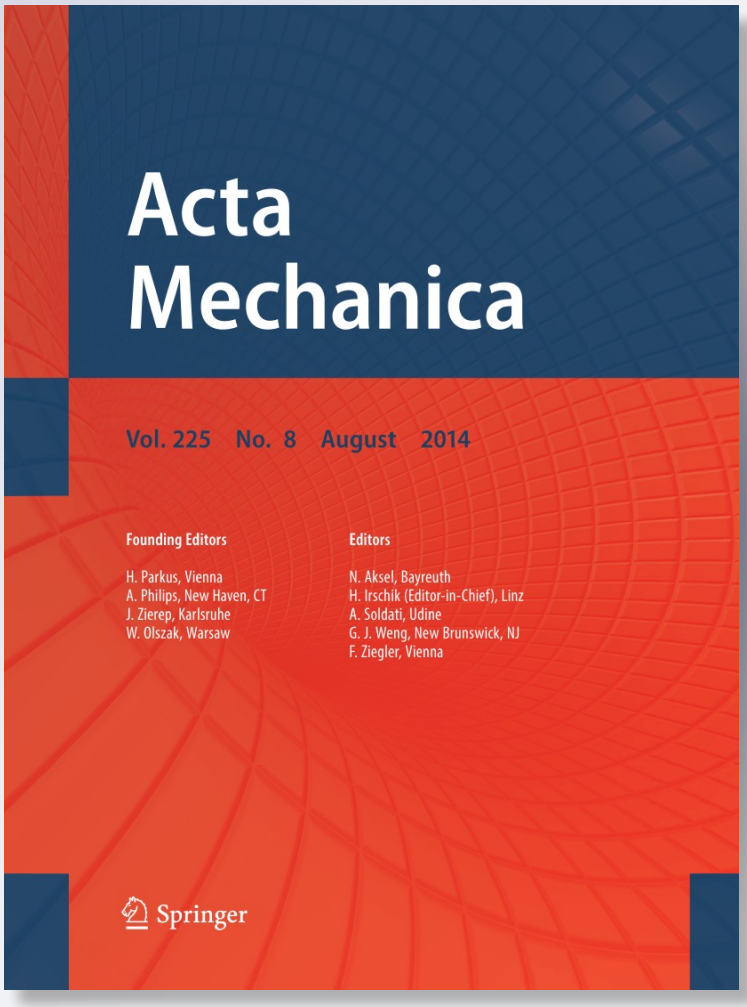

Springer

Acta Mech 225, 2423–2434 (2014)
DOI 10.1007/s00707-014-1126-0

Shiva P. Pudasaini

Dynamics of submarine debris flow and tsunami

Received: 27 February 2013 / Revised: 7 October 2013 / Published online: 31 May 2014

Abstract The general two-phase debris flow model proposed by Pudasaini (J. Geophys. Res. 117:F03010, 2012, doi:10.1029/2011JF002186) is employed to simulate subaerial and submarine two-phase debris flows and the mechanics of complex wave generation and interactions between the solid and the fluid phases. This includes the fluid waves or the tsunami generated by the debris impact at reservoirs, lakes, and oceans. The analysis describes the generation, amplification, and propagation of super tsunami waves and run-ups along coastlines, debris slide and deposition at the bottom floor, and debris shock waves. Accurate and advance knowledge of the arrival of tsunami waves in the coastal regions is very important for the design of early warning strategies. Here, we show that the amount of solid grain in the fluid reservoir plays a significant role in controlling the overall dynamics of the submarine debris flow and the tsunami. For very small solid particle concentrations in the reservoir, the submarine debris flow moves significantly faster than the surface tsunami wave. As the solid volume fraction in the reservoir increases, the submarine debris speed slows down. For relatively large solid volume fractions in the reservoir, the speed of the submarine debris becomes slower than the surface tsunami wave. This information can be useful for early warning strategies in the coastal regions. The fast or slow speed of the submarine wave can be attributed to several dynamical aspects of the model including the generalized drag, basal traction, pressure gradient, virtual mass force, the non-Newtonian viscous stress, and the strong phase interaction between the solid and the fluid as they enhance or diminish the motion of the solid phase. Solid particle concentration in the reservoir dam also substantially influences the interaction between the submarine debris flow and the frontal wall of the dam, and the interaction between the tsunami and the submarine debris wave. The tsunami wave impact generates a largely amplified fluid level at the dam wall. Submarine debris shock waves are observed for small solid volume fractions in the reservoir. Another important aspect of the simulation is to investigate the complex interactions between the internal submarine debris wave and the surface tsunami wave. Three complex waves occur simultaneously: the subaerial debris flow in the upstream region, submarine debris flow in the reservoir basin, and a super tsunami wave on the surface of the reservoir. This helps to develop insight into the basic features of the complex nonlinear solid and fluid waves and their interactions.

1 Introduction

Subaerial and submarine landslides and debris flows are very important sediment transport mechanisms. Examples include sediment transport in hill slopes, in hydraulic reservoirs and channels, and in submarine environments. These are effectively two-phase flows of solid particles mixed with fluid. Accurate knowledge

Presented at the 8th European Solid Mechanics Conference in the Graz University of Technology, Austria, 9–13 July 2012.

S. P. Pudasaini (✉)
Department of Geodynamics and Geophysics, Steinmann Institute,
University of Bonn, Meckenheimer Allee 176, 53115 Bonn, Germany
E-mail: pudasaini@geo.uni-bonn.de

of the distribution and evolution of the solid and the fluid phases is very important from the environmental and industrial point of view, including the huge landslides in the coastal areas and particle transport in hydroelectric power plants.

Submarine landslides are commonly observed huge mass-wasting processes. They constitute one of the most important mechanisms for sediment movement from shallow to deep-marine environments, and in shaping continental margins. Examples include the Mauritania Slide Complex, which is one of the largest events on the Atlantic margin (area $\sim$30,000 km^2, volume 600 km^3, run-out 300 km; [3,10,18]). Even larger slides are the giant Storegga Slide (95,000 km^2), the Saharan Debris flow (48,000 km^2), and the Canary Slide (40,000 km^2) with volume $\sim$1,000 km^3 [3,14,22,25]. Characteristically, these mass-wasting processes are giant, take place on gentle slopes, and run exceptionally long distances [46]. Another important scenario is the subaerial debris flows hitting the fluid environments. For example, the large 3700 B.P. Eibsee rock-ice avalanche (4×10^8 m^3 in volume) in Zugspitze (where the rock-ice avalanche plunged into Eibsee) entrained water and lake sediment and largely turned into a debris flow [2,20]. This could have generated water waves (tsunami) in the Eibsee (lake) and the subsequent debris flood. The Zugspitze may potentially fail again with large volume and unexpectedly run over a long propagation distance.

There are several hazards and socioeconomic aspects related to submarine landslides: (i) More than 40 % of the world's population is living within 100 km of the coast [10,26]. Submarine slides may trigger destructive tsunamis and catastrophically affect coastal population [13,25,28,51]. Assessing the extent of mass movement at continental margins is important to evaluate risks for offshore constructions and coastal communities [17]. Although recently research has been focused toward evaluating the tsunami generation and risks [8,15,16,53], not much is known about tsunami deposits. (ii) Some of the slide complexes are situated on oil and gas fields [10]. Submarine canyons store and conduct terrestrial clastic sediments into deep-marine environments and play a major role for hydrocarbon reservoirs [35,36]. (iii) There is a direct threat to submarine installations, including oil platforms, pipelines, cables, and wind installations. These offshore resource exploitations and constructions require detailed hazard assessments for engineering and environmental projects. Oil industries, hydrocarbon exploration, and production activities have recently been moved further into deep water [11,23]. They are further interested in studying submarine slides because slides are capable of modifying the architectural and sedimentological characteristics of submarine channels and levees as they are often connected to potential deep-sea hydrocarbon reservoirs [3]. Therefore, the societal interest is increasing on mapping, modeling, and simulation of submarine landslides [10].

Due to geophysical, geological, geotechnical, environmental, and cultural importance, considerable attention has been drawn in the past to investigate the mechanism of slope failure and movements, material properties, modeling, numerical simulations, debris impact, tsunami generation, inundation, and associated mitigation strategies. Examples include the 1958 Lituya Bay Megatsunami (Alaska) generated by an earthquake-induced landslide [30] and the 1963 Vajont landslide (Italy) induced megatsunami [31]. However, due to multiple complexities, these events are still poorly understood in terms of dimensions, phases, and mechanics. Debris flows and induced super tsunamis are extremely destructive and dangerous natural hazards [52,54]. So, there is a significant need for reliable methods for predicting the dynamics, the run-out distances, and the inundation areas of such events as well as prevention and reduction in such disasters, including their socioeconomic aspects. On the one hand, existing studies mainly concentrate on the description of the slide and depositional processes [10,13]. On the other hand, modeling and simulation of tsunami triggered by landslides, run-ups, and inundation is still an emerging field and different modeling approaches may lead to very different results [43–45].

Subaerial and submarine debris flows are multi-phase, gravity-driven flows consisting of a broad distribution of grain sizes mixed with fluid. The rheology and flow behavior vary depending on the sediment composition and the percentage of solid and fluid phases. Research in previous decades and recent years focused on different aspects of single- and two-phase debris avalanches and debris flows and induced tsunami [1,4,7,12,19,21,24,33,37–39,42,48,49,52,54], which was recently advanced by Pudasaini [43] with a comprehensive theory that accounts for interactions between the solid and the fluid. The model, which includes buoyancy, also includes three new and important dominant physical aspects of solid-volume-fraction-gradient-enhanced non-Newtonian viscous stress, virtual mass, and generalized drag. This model constitutes the most generalized two-phase flow model to date and can reproduce results from most previous simple models that considered single- and two-phase avalanches and debris flows as special cases [19,37,39,48]. The two-phase model has been applied to simulate flows of debris mixture sliding down an inclined channel that extends to the horizontal run-out [43–45].

Here, we advance further by primarily focusing on another very important aspect of two-phase mass flows: We systematically analyze the effects of the solid volume fraction in the fluid (water) reservoir on the dynamics of the submarine debris flow, sediment transport, and tsunami waves. This helps to develop insight into the basic features of the complex nonlinear solid and fluid waves and their interactions. Here, we focus primarily on the complex dynamics of a two-phase subaerial debris flow sliding down an inclined channel plunging into a quiescent fluid reservoir with different solid concentrations with particular emphasis on the dynamics of the submarine debris flow with respect to the available and changing volume fraction of the solid in the reservoir. Another important aspect of the simulation is to investigate the complex interactions between the internal submarine debris wave and the surface tsunami. The results demonstrate that the general two-phase debris flow models are able to adequately describe the complex dynamics of two-phase subaerial debris flows; particle-laden and dispersive flows; sediment transports; debris-induced tsunamis and submarine debris flows; turbidity currents and associated sophisticated phenomena including the solid and fluid waves and their complex interactions and dynamic impacts. Our findings add substantial and fundamental values for the dynamical understanding of complex multi-phase systems and flows, proper modeling of run-out distances, geomorphological interpretation of past events, and hazard prediction and mitigation in debris flow and debris avalanche prone mountain slopes.

2 The two-phase solid–fluid mixture mass flow model

The general two-phase model (Pudasaini, 2012) [43] is briefly presented here. The model includes many of the essential physical phenomena. It employs the Mohr–Coulomb plasticity for the solid stress, and the fluid extra stress is modeled as a non-Newtonian viscous stress that is enhanced by the solid volume fraction gradient. The generalized interfacial momentum transfer is modeled by including the force on the particulate phase due to viscous drag, buoyancy, and the relative acceleration between the solid particles and the fluid (the virtual mass). The Richardson and Zaki relationship for the terminal velocity of a solid particle falling in the fluid and the Kozeny–Carman expression for fluid flows through densely packed grains are combined to develop a new generalized drag force, which is expressed explicitly in terms of several essential physical parameters. This drag force reveals the most basic features of the flow, covers both the solid-like and fluid-like contributions in the mixture, and can be applied to problems ranging from linear to quadratic drags at low and high velocities. The new two-phase debris flow model is presented in a well-structured conservative hyperbolic–parabolic form. There are strong couplings between the solid and the fluid momentum transfer, both through the interfacial momentum transfer and the enhanced viscous fluid stresses. Strong phase interactions lead to simultaneous deformation of the solid and the fluid phases, and mixing and separation between phases. Inclusion of the non-Newtonian viscous stresses is important in several aspects. The evolution, advection, and diffusion of the solid volume fraction as a field variable play an important role. The approach, applicabilities, and limitations of the model in connection to the existing models are extensively discussed in Pudasaini [43].

For simplicity, here, we consider the general two-phase debris flow model [43] reduced to one-dimensional channel flows. For the structure of the one-dimensional model used below, see Appendix D in Pudasaini [43]. The depth-averaged mass and momentum conservation equations for the solid and fluid phases are:

$$\frac{\partial}{\partial t}(\alpha_s h) + \frac{\partial}{\partial x}(\alpha_s h u_s) = 0, \quad \frac{\partial}{\partial t}(\alpha_f h) + \frac{\partial}{\partial x}(\alpha_f h u_f) = 0, \tag{1}$$

$$\frac{\partial}{\partial t}\left[\alpha_s h\left(u_s - \gamma\, C\left(u_f - u_s\right)\right)\right] + \frac{\partial}{\partial x}\left[\alpha_s h\left(u_s^2 - \gamma\, C\left(u_f^2 - u_s^2\right) + \beta_s \frac{h}{2}\right)\right] = h S_s, \tag{2}$$

$$\frac{\partial}{\partial t}\left[\alpha_f h\left(u_f + \frac{\alpha_s}{\alpha_f} C\left(u_f - u_s\right)\right)\right] + \frac{\partial}{\partial x}\left[\alpha_f h\left(u_f^2 + \frac{\alpha_s}{\alpha_f} C\left(u_f^2 - u_s^2\right) + \beta_f \frac{h}{2}\right)\right] = h S_f, \tag{3}$$

in which $\beta_s = \varepsilon K p_{b_s}$, $\beta_f = \varepsilon p_{b_f}$, $p_{b_f} = -g^z$, $p_{b_s} = (1-\gamma) p_{b_f}$. In (2)–(3) the source terms are

$$S_s = \alpha_s\left[g^x - \frac{u_s}{|u_s|}\tan\delta p_{b_s} - \varepsilon p_{b_s}\frac{\partial b}{\partial x}\right] - \varepsilon\alpha_s\gamma p_{b_f}\left[\frac{\partial h}{\partial x} + \frac{\partial b}{\partial x}\right] + C_{DG}\left(u_f - u_s\right)|u_f - u_s|^{J-1}, \tag{4}$$

$$S_f = \alpha_f \Bigg[g^x - \varepsilon \Bigg[\frac{1}{2} p_{b_f} \frac{h}{\alpha_f} \frac{\partial \alpha_s}{\partial x} + p_{b_f} \frac{\partial b}{\partial x} - \frac{1}{\alpha_f N_R} \left\{ 2 \frac{\partial^2 u_f}{\partial x^2} - \frac{\chi u_f}{\varepsilon^2 h^2} \right\}$$

$$+ \frac{1}{\alpha_f N_{R_A}} \left\{ 2 \frac{\partial}{\partial x} \left(\frac{\partial \alpha_s}{\partial x} \left(u_f - u_s \right) \right) \right\} - \frac{\xi \alpha_s \left(u_f - u_s \right)}{\varepsilon^2 \alpha_f N_{R_A} h^2} \Bigg] \Bigg] - \frac{1}{\gamma} C_{DG} \left(u_f - u_s \right) |u_f - u_s|^{J-1}, \quad (5)$$

where

$$C_{DG} = \frac{\alpha_s \alpha_f (1-\gamma)}{\left[\varepsilon U_T \{ P F(Re_p) + (1-P) G(Re_p) \} \right]^J}, \quad F = \frac{\gamma}{180} \left(\alpha_f / \alpha_s \right)^3 Re_p, \quad G = \alpha_f^{M(Re_p)-1},$$

$$\gamma = \frac{\rho_f}{\rho_s}, \quad Re_p = \frac{\rho_f d \, U_T}{\eta_f}, \quad N_R = \frac{\sqrt{gL} H \rho_f}{\alpha_f \eta_f}, N_{R_A} = \frac{\sqrt{gL} H \rho_f}{A \eta_f}. \quad (6)$$

Here, x and z are coordinates along the flow directions, and g^x and g^z are the components of gravitational acceleration. The solid and fluid constituents are denoted by s and f, h is the flow depth, and u_s and u_f are the solid and fluid velocities. ρ_s, ρ_f, and α_s, α_f denote the densities and volume fractions of the solid and the fluid, respectively, with the constraint $\alpha_s + \alpha_f = 1$. L and H are the typical length and depth of the flow, $\varepsilon = H/L$ is the aspect ratio, and $\mu = \tan\delta$ is the basal friction coefficient. K is the earth pressure coefficient (function of δ and ϕ, which are the basal and internal friction angles of solid), C_{DG} is the generalized drag coefficient, $J = 1$ or 2 represents linear or quadratic drag. U_T is the terminal velocity of a particle and $P \in [0, 1]$ is a parameter which combines the solid-like (G) and fluid-like (F) drag contributions to flow resistance. p_{b_f} and p_{b_s} are the effective fluid and solid pressures. γ is the density ratio, C is the virtual mass coefficient (solid particles induced kinetic energy of fluid phase), η_f is the fluid viscosity, M is a function of the particle Reynolds number (Re_p), χ includes vertical shearing of fluid velocity, and ξ takes into account different distributions of α_s. $A = A(\alpha_f)$ is the mobility of the fluid at the interface, and N_R and N_{R_A} are Reynolds numbers associated with the classical Newtonian and enhanced non-Newtonian fluid viscous stresses. Slope and channel topography are represented by $b = b(x)$.

There are two important aspects of the model equations. First, the inertial terms on the left hand side of (2)–(3) include the lateral pressure (associated with β_s and β_f) and the virtual mass, C. Secondly, the source in the solid momentum (4) has three different contributions from (i) gravity, the Coulomb friction and the slope gradient (first square bracket); (ii) terms associated with the buoyancy force (second square bracket); and (iii) the generalized drag contribution (C_{DG}) (last term). The source term for the fluid momentum equation (5) has six different contributions; the first three terms emerge from the gravity load (first term), the fluid pressure gradient at the bed (second term), and the fluid pressure applied to the topographic gradient (third term). The fourth and fifth group of terms associated with N_R and N_{R_A} are the Newtonian viscous and the solid-volume-fraction-gradient-enhanced non-Newtonian viscous stresses, respectively. The non-dimensional number N_{R_A} is termed as the mobility number [43–45]. Finally, the last term is due to the drag force. The term associated with β_s in (2) accounts for the buoyancy-reduced lateral pressure. The solid load is reduced by the buoyancy force by the factor $(1-\gamma)$ as seen in p_{b_s}, Coulomb friction, and in the drag term, C_{DG}. Here, we are mainly focusing our attention on the dynamics of submarine debris flows and surface tsunami waves with respect to the available and changing solid volume fraction (α_s) in the reservoir or in the fluid environment. It is important to note that α_s appears globally as a field variable in the model equations (1)–(6).

3 Numerical method, physical parameters and simulation set-up

The model equations (1)–(3) are written as a set of well-structured, nonlinear hyperbolic–parabolic partial differential equations in conservative form with complex source terms (4)–(5). This facilitates numerical integration even when shocks are formed in the field variables [39,41,42]. The model equations are solved in conservative variables $\mathbf{W} = \left(h_s, h_f, m_s, m_f \right)^t$, where $h_s = \alpha_s h$, $h_f = \alpha_f h$ are the solid and fluid contributions to the debris height; and $m_s = \alpha_s h u_s$, $m_f = \alpha_f h u_f$, are the solid and fluid momentum fluxes [43]. As $h_s + h_f = h$, this definition of the conservative variables automatically satisfies the condition $\alpha_s + \alpha_f = 1$. The high-resolution shock-capturing Total Variation Diminishing Non-Oscillatory Central (TVD-NOC) scheme is implemented [34,40,50]. We consider a two-phase subaerial debris flow that hits a

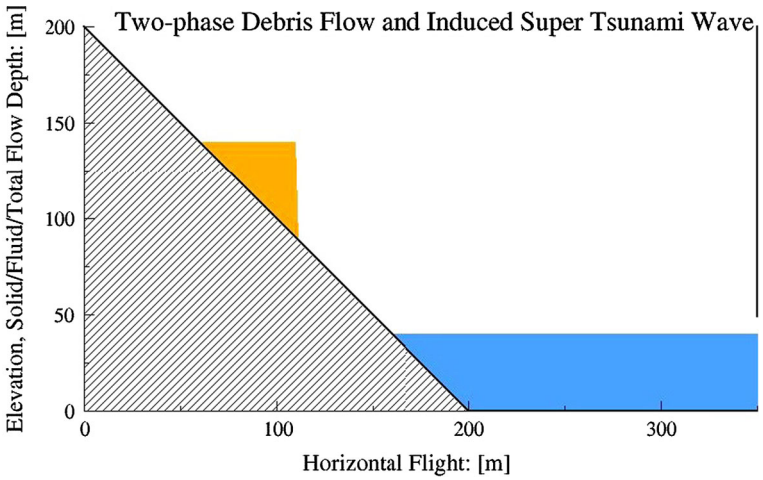

Fig. 1 Initial debris mass (in *triangle*) and the quiescent reservoir. The initial debris consists of 50 % solid and 50 % fluid that is mixed homogeneously. The *orange* and *blue colors* indicate the volume fractions of the solid and the fluid. At $t = 0$ s, only the solid (*orange*) is seen while the fluid (*blue*) is on the back side of the solid in the triangle. Three different initial amounts of the solid particles in the reservoir are assumed in the simulation: $\alpha_s = 0$, 2 and 10 % (color figure online)

quiescent fluid reservoir downstream (Fig. 1) which is also an integral part of the whole model system. The upper part of the channel is inclined ($\zeta = 45°$) followed by a horizontal reservoir with a dam wall in the distal front. The initial triangle is uniformly filled with a homogeneous mixture of 50 % solid and 50 % fluid. The reservoir consists of different amounts of solid grains ranging from 0–10 %. The parameter values are: $\phi = 35°$, $\delta = 15°$, $\rho_f = 1{,}100\text{kgm}^{-3}$, $\rho_s = 2{,}500\text{kgm}^{-3}$, $N_R = 150{,}000$, $N_{R_A} = 30$, $Re_p = 1$, $U_T = 1$, $P = 0.5$, $J = 1$, $\chi = 3$, and $\xi = 5$. Following Rivero et al. [47], Maxey and Riley [27] and Pudasaini [43] we take $C = 0.5$. The selection of these parameters is mentioned in Pudasaini [43] and is mainly based on field and laboratory data. These are physical parameters associated with the mixture material, e.g., the true densities of the solid and the fluid constituents and the flow dynamics. Thus, these parameter values are assumed to be suitable both for the subaerial and submarine two-phase debris flows.

We apply the model to simple, one-dimensional debris flow, tsunami generation and propagation. The idea to use a setting as in Fig. 1 is to study in detail the complex interactions of the submarine debris motion and tsunami wave within the fluid reservoir, and with the front wall. This helps to quantify the arrival time of the debris and the tsunami, and tsunami height. With this information, we can optimally construct the frontal part of the dam (e.g., the vertical wall as considered here, or other type of structure, including a triangular one as appropriate) to control the tsunami wave and debris material inside the reservoir and beyond the dam, and perhaps most importantly, to estimate the strength of the dam to withstand the huge dynamic impact of the megatsunami suddenly induced by landslide impact at the reservoir and its subsequent subaqueous motion. The analysis also includes the impact at the dam wall by the dense and rapid submarine debris flow. It has important applications in aquatic environments and hydro-power generating plants in connection to the particle transport in the fluid, and the erosion due to particle impact at the turbines.

4 Simulation results

The model analysis includes the generation and interactions of debris and fluid waves. The state of the solid volume fraction is essential for the correct prediction of the turbidity currents, sediment transport, and deposition in the subaerial and submarine environments. Figure 1 shows the initial configuration. As the two-phase subaerial debris flow hits a quiescent fluid reservoir (no grains in the reservoir), a tsunami wave is generated, and a submarine debris wave continues to slide (Fig. 2). At $t = 2$ s, the debris hits the reservoir dam to generate a tsunami. The debris mass slides down the slope as a submarine debris flow and the tsunami wave propagates to the right. As the debris continues to hit the reservoir with higher momentum, the tsunami wave is amplified and more and more fluid mass from the left of the reservoir is pushed to the right. This results in a hydrodynamic impact vacuum, or crater [32,45], which increases in time and continues for quite a while. At $t = 3$ s, the submarine debris hits the horizontal basin of the dam reservoir, and the tsunami becomes a

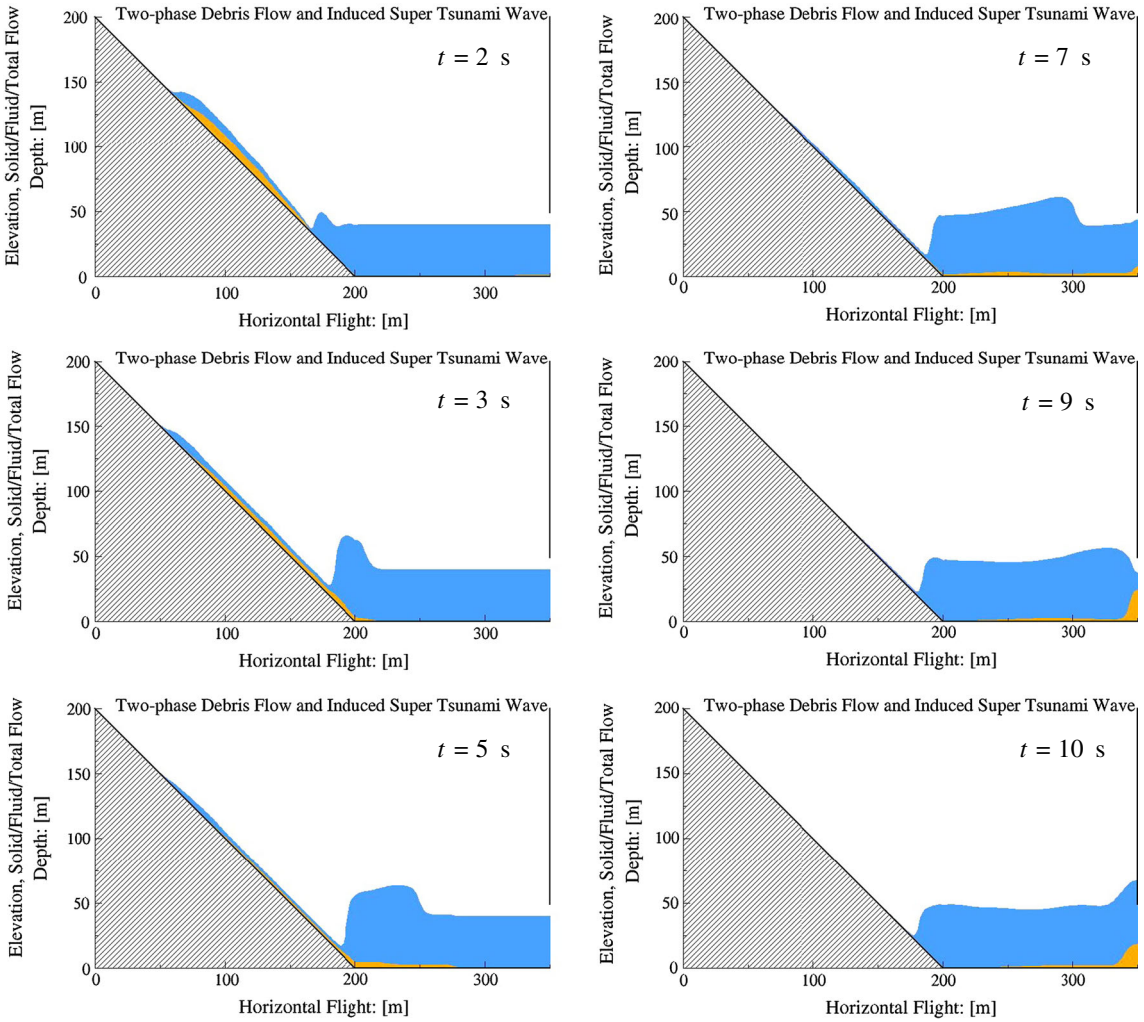

Fig. 2 Two-phase subaerial debris flow hits a fluid reservoir at $t = 2$ s, generates a tsunami wave, and a submarine debris wave continues to slide down. *Orange* and *blue colors* indicate volume fractions of solid and fluid. Initially, $\alpha_s = 0$ in the reservoir, and the initial debris mass consists of 50 % solid and 50 % fluid. At $t = 3$ s, the tsunami wave is amplified, leading to an increasing hydrodynamic impact vacuum. There are three complex flows taking place simultaneously: a subaerial debris flow in the upstream, a submarine debris flow in the downstream and at the reservoir floor, and a surface tsunami wave. At $t = 3$ s, the submarine debris hits the horizontal basin of the reservoir dam and the tsunami becomes a super wave. At $t = 5$ s, the submarine debris wave is moving much faster than the tsunami wave. At $t = 7$ s, a left-going water wave starts and the hydrodynamic vacuum is decreasing. A particularly important observation is that the submarine debris already hits the right wall of the dam, but the tsunami is still following the debris mass. This time gap can be used in generating early warning signals. At $t = 9$ s, the submarine debris hits the distal dam wall and a shock wave of debris material is generated that propagates upstream. At $t = 10$ s, the tsunami also hits the distal dam wall (color figure online)

super wave. Three complex flows occur simultaneously: (i) a subaerial debris flow in the upstream region, (ii) a submarine debris flow in the downstream and in the reservoir basin, and (iii) a super tsunami wave on the surface of the reservoir. At $t = 5$ s, it is clearly seen that the submarine debris wave (internal wave) is moving much faster than the free-surface tsunami. At $t = 7$ s, the debris mass supply from the upstream is exhausted so that a left-going water wave starts and slowly moves back to the slope side. Then, the height of the left side of the tsunami wave is diminished and decreases the hydrodynamic vacuum [45]. Four clearly observable waves exist at this moment; two tsunami waves with one toward the right and another toward the left, and two waves associated with the submarine debris flow, one at the front and another at the tail. A particularly important observation is that, at $t = 7$ s, the submarine debris flow has already hit the distal vertical wall of the dam, but the tsunami is still following it. As soon as the debris hits the dam wall ($t = 9$ s), a shock wave of debris material is generated and propagates upstream. At some later time ($t = 10$ s), the submarine

debris shock wave is diffused (as the tsunami wave also hits the right wall of the dam and runs-up). After a long time, the fluid level in the dam becomes (almost) horizontal (not shown). This behavior should be an observable natural phenomenon and was simulated for the first time by Pudasaini and Miller [45] by using a real two-phase flow model with a high-resolution shock-capturing scheme. The observed time gap between the submarine debris flow and the tsunami hitting the distal wall ($t = 7$ s) may potentially be used to generate an early warning signal. In the present relatively small scale simulation, the time gap is on the order of 2 s, which in natural scale flows is expected to be on the order of some seconds, or minutes, or even more. In the context of a hydro-power generating reservoir, this may already play a crucial role for the integrity of the reservoir dam as some extra safety measures can immediately be applied, e.g., by shutting down the power generating plant, or by diverting the flow to other safe directions and by opening or closing some extra lock gates. This, however, may depend, e.g., on the geometry of the basin, flow configuration, and the flow dynamics.

The debris impact produces a tsunami wave while at the same time it generates a submarine debris flow along the reservoir basin. Simulation results show that the amount of solid grain (in the form of sand, clay, gravel, etc.) in the dam plays a significant role in controlling the overall dynamics of the tsunami wave and the submarine debris flow. For very small solid particle concentrations in the reservoir, the submarine debris flow moves significantly faster than the surface tsunami. As the solid volume fraction in the reservoir increases, the submarine debris speed slows down. For relatively larger values of the solid volume fraction in the reservoir, the speed of the submarine debris becomes slower than the surface tsunami. Such a potentially observable natural phenomenon has been demonstrated here for the first time by applying the real two-phase solid–fluid mixture mass flow model [43] as follows.

More important observations are presented in Fig. 3. This figure shows that the amount of the solid particles in the reservoir strongly controls the overall dynamics of the submarine debris flow. Solutions are plotted for different times and different concentrations of the solid in the reservoir. The left and right panels are simulations for time $t = 3$ s and $t = 5$ s, respectively. The left panels ($t = 3$ s) show the moment when the submarine debris hits the bottom floor of the fluid reservoir with or without solid grains. The top, middle, and the bottom rows are simulated with the different solid concentrations in the reservoir: $\alpha_s = 0, 2, 10\,\%$, respectively. The top, middle, and bottom panels in the right column ($t = 5$ s) show that the front of the submarine debris flow moves fastest for $\alpha_s = 0\,\%$, while the submarine debris front is slowest for $\alpha_s = 10\,\%$. The front of the submarine debris with $\alpha_s = 2\,\%$ lies in between. Another important aspect is the arrival time between the tsunami and the submarine wave. For the top right panel for which the reservoir consists of pure water ($\alpha_s = 0\,\%$), the submarine debris wave is far ahead of the surface tsunami wave, while in the middle right panel, for which the reservoir consists of little amount of solid grain ($\alpha_s = 2\,\%$), the submarine wave is still ahead of the tsunami wave. However, the gap between the submarine debris wave front and the front of the tsunami wave has been decreased as compared to the former. The bottom right panel represents the simulation with relatively larger amount of the solid grains in the reservoir ($\alpha_s = 10\,\%$). The dynamics has now been changed substantially. For this, both the submarine debris wave and the surface tsunami wave move almost at the same speed. For an even larger amount of the solid in the dam ($\alpha_s > 10\,\%$), the tsunami would dominate the submarine debris wave. This analysis indicates that the amount of solid grain in the reservoir is crucial to control the dynamics of the submarine landslide and the debris impact generated tsunami wave.

A relatively long-time behavior, the interaction of the submarine debris wave and the tsunami wave with the frontal dam wall, and the interaction between the debris and the tsunami wave are presented in Fig. 4. Here, simulation results clearly indicate that the amount of the solid particles in the dam controls not only the dynamics of the submarine debris flow but also the dynamics of the tsunami. Solid particle concentration in the reservoir also substantially influences the interaction between the submarine debris flow and the frontal wall of the dam, and the interaction between the tsunami and the submarine debris wave. The left and right panels are simulations for time $t = 7$ s and $t = 9$ s, respectively. The top, middle, and the bottom rows are simulated with the different solid concentrations in the reservoir: $\alpha_s = 0, 2, 10\,\%$, respectively. The top, middle, and bottom panels in the left column ($t = 7$ s) show that the front of the submarine debris flow moves fastest for $\alpha_s = 0\,\%$, while the submarine debris front is slowest for $\alpha_s = 10\,\%$. The front of the submarine debris with $\alpha_s = 2\,\%$ lies in between. Debris shock waves are observed in the right column ($t = 9$ s) for $\alpha_s = 0$ and $2\,\%$. However, for $\alpha_s = 10\,\%$, a submarine debris shock wave does not exist, because, the larger amount of the grain in the reservoir is able to diffuse the sharp front of the debris propagation, the front motion is diffused and slowed down. So, not enough energy was available for the shock structure to be formed as in the upper two panels. The lower right panel shows how the tsunami impact could generate a largely amplified fluid level at the dam wall. This implies the necessity of considering the possible huge dynamic impact generated by the tsunami that could be induced by landslides while constructing a dam of a reservoir, e.g., for hydro-power

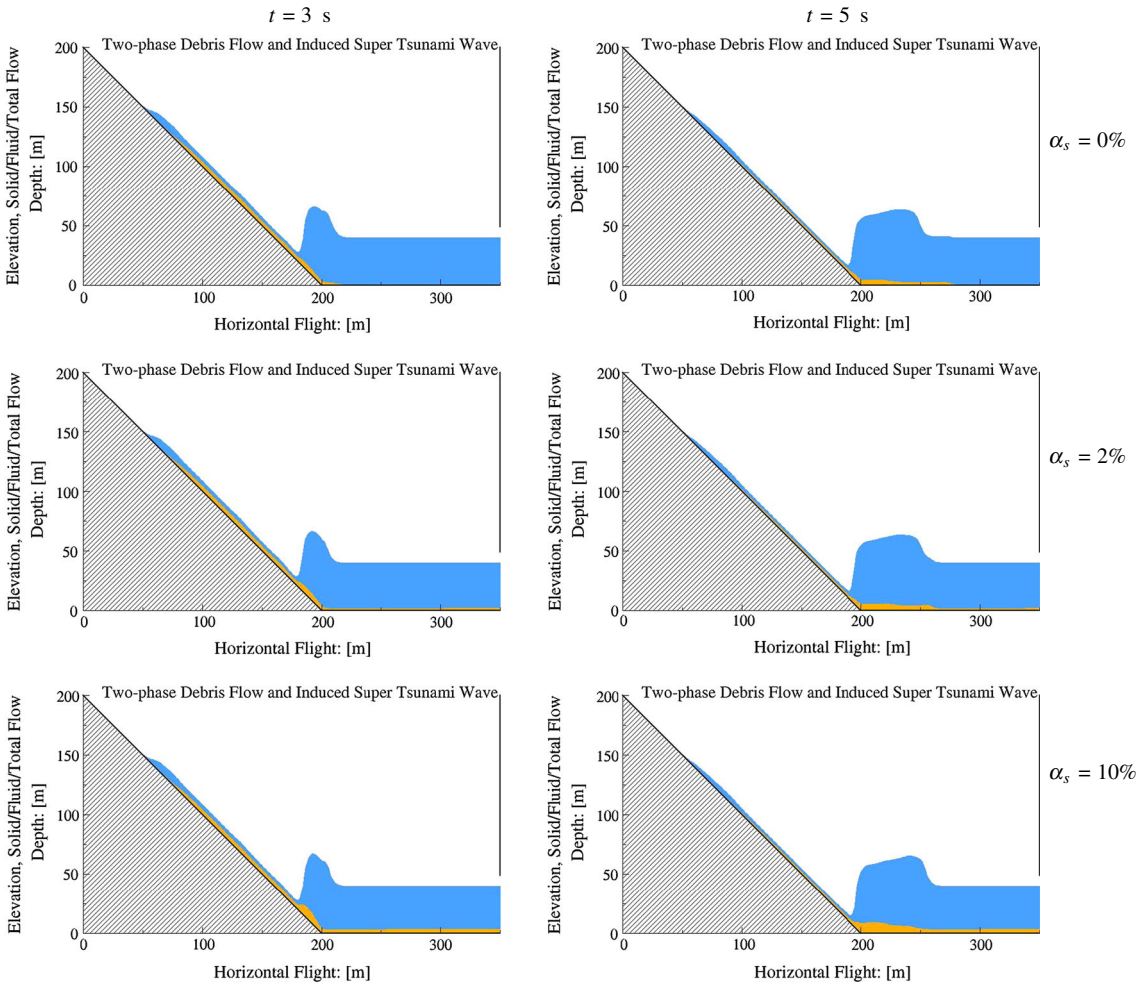

Fig. 3 Amount of the solid particles in the reservoir controls the dynamics of the submarine debris flow. The *left* and *right panels* are simulations for time $t = 3$ s and $t = 5$ s, respectively. The *top*, *middle* and the *bottom rows* are simulated with the different solid concentrations in the reservoir: $\alpha_s = 0, 2, 10\,\%$, respectively. The *top*, *middle*, and *bottom panels in the right column* ($t = 5$ s) show that the front of the submarine debris flow moves fastest (also compare with the front of the tsunami) for $\alpha_s = 0\,\%$, while the submarine debris front is slowest for $\alpha_s = 10\,\%$. The front of the submarine debris with $\alpha_s = 2\,\%$ lines in between

generation. The dam safety can thus be better estimated by the present real two-phase flow simulation which simultaneously describes the interactions of the dam with the submarine debris and the surface tsunami waves in a unified way.

5 Discussion

The general two-phase debris flow model (Pudasaini, 2012) [43] includes three fundamentally new and dominant physical aspects such as enhanced viscous stress, virtual mass, and generalized drag (in addition to buoyancy). It constitutes the most generalized two-phase flow model to date. The advantage of this two-phase debris flow model over classical single-phase or quasi-two-phase models is that the initial mass can be divided into several parts by appropriately considering the solid volume fraction. These parts include a dry (landslide or rock slide), a fluid (water or muddy water; e.g., reservoirs and rivers), and a general debris mixture material as needed in real flow simulations. This innovative formulation provides an opportunity to simultaneously simulate (within a single framework) the sliding debris (or landslide), the water lake or ocean, the debris impact at the lake or ocean, the tsunami generation and propagation, the mixing and separation between the solid and fluid phases, and the sediment transport and deposition process in the bathymetric surface. Applications of this model include: sediment transport on hill slopes, river streams, hydraulic channels (e.g., hydro-power

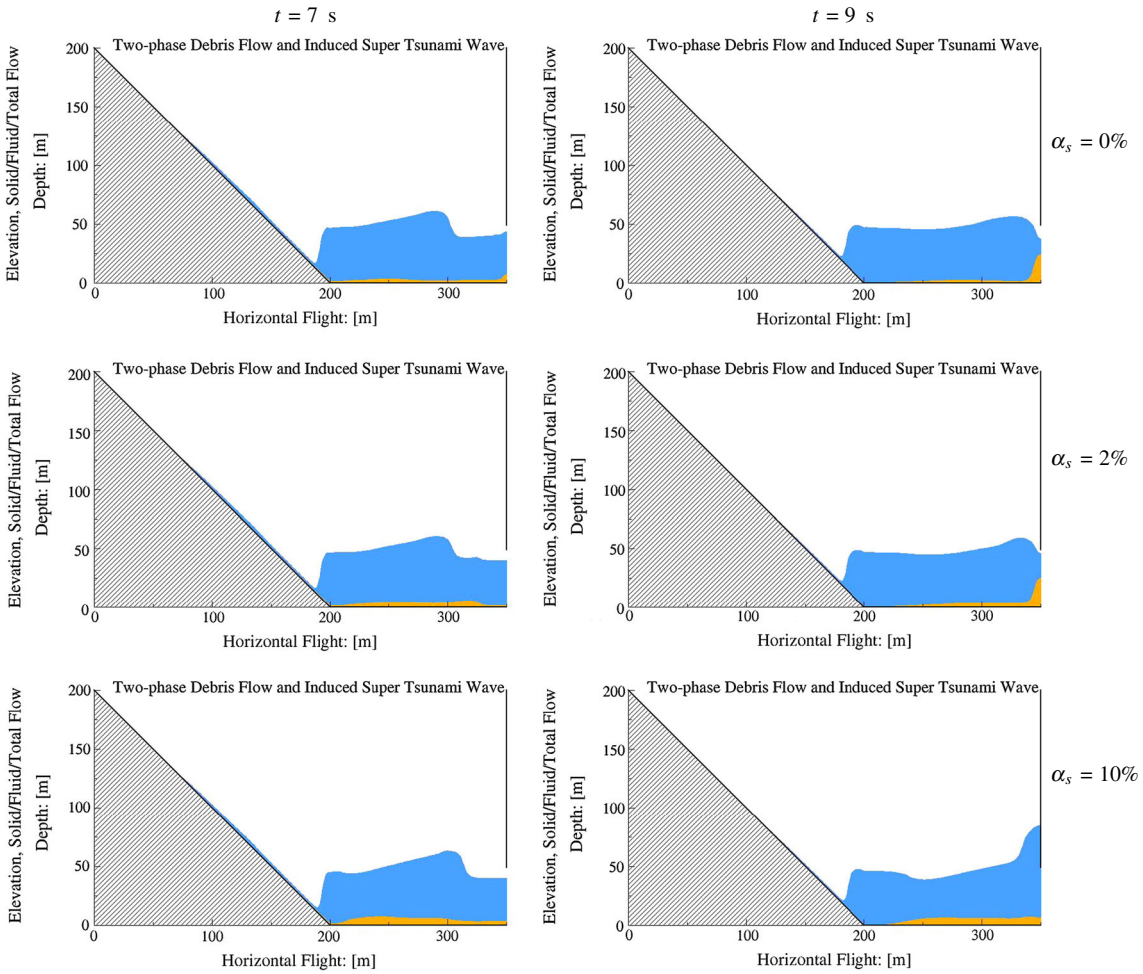

Fig. 4 Same as in Fig. 3, but now for larger time. Here, the simulation results clearly indicate that the amount of the solid particles in the reservoir controls both the dynamics of the submarine debris flow and the dynamics of the tsunami wave. Solid particle concentration in the reservoir also substantially influences the interaction between the submarine debris flow and the frontal wall of the dam, and the interaction between the tsunami and the submarine debris wave. The *top*, *middle*, and *bottom panels in the right column* ($t = 9$ s) show that the front of the submarine debris flow moves fastest for $\alpha_s = 0\,\%$, while the submarine debris front is slowest for $\alpha_s = 10\,\%$ (also compare with the tsunami front). The front of the submarine debris with $\alpha_s = 2\,\%$ lies in between. Debris shock waves are observed for $\alpha_s = 0$ and $2\,\%$. However, for $\alpha_s = 10\,\%$, the submarine debris shock wave does not exist. Because the larger amount of the grain in the reservoir is able to diffuse the sharp front of the debris propagation where the front motion is slowed down. Energy loss in diffusion prevented from forming shock structure as seen in the upper two panels

reservoirs and plants); lakes, fjords, coastal lines, and aquatic ecology; and submarine debris impact and the rupture of submarine fiber optic, cables and pipelines along the ocean floor, and damage to offshore drilling platforms. Numerical simulations reveal that the dynamics of debris impact induced tsunamis in mountain lakes or oceans are fundamentally different than the tsunami generated by pure rock avalanches and landslides [7,54]. One of the reasons for this is that rock avalanches and landslides are relatively dry, and landslides typically do not tend to shear largely. However, debris flows are largely mixed with water and may substantially deform. Another important aspect is that, depending on the degree of saturation and the amount of the fluid in the debris, as soon as the debris mass impacts the fluid reservoir, either fluid will tend to separate from the debris and be a part of the reservoir (if, say the impacting debris contains fluid more than it is needed for full saturation), or if the impacting debris contains fluid below saturation limit (or if the debris is relatively loose and dry), fluid from the reservoir can infiltrate into the debris. The tsunami generation mechanism is also dependent on the state of the intactness or dispersion of the impacting debris. For a real two-phase debris flow, the main points are the complex phase interactions, intermixing, and dispersion characteristics. This is in contrast to the largely single-phase characteristics of landslides and rock avalanches when it is concerned with

the interaction of a mass flow with a fluid reservoir, during the impact and/or when the debris moves in the submarine environment. The analysis includes the generation, amplification, and propagation of super tsunami waves and run-ups along coastlines, debris slide and deposition at the bottom floor, and debris shock waves. It is observed that the submarine debris speed can be faster than the tsunami speed. This information can be useful for early warning strategies in coastal regions. These findings substantially increase our understanding of complex multi-physics systems and multi-phase flows. Furthermore, they allow for the proper modeling of landslide- and debris-induced tsunami, the dynamics of turbidity currents and sediment transport, and the associated applications to hazard mitigation, geomorphology, and sedimentology.

A fundamental question now is: why does the submarine debris flow move faster than the tsunami for relatively smaller amount of the solid particles in the reservoir downstream? This can be attributed to several dynamical aspects of the model. One of the most important aspects of the new two-phase model is the influence of the generalized drag, C_{DG}. The drag increases with the increasing amount of the grain. This can be the main reason for why the submarine debris moves faster than the tsunami for a smaller amount of the solid grain in the reservoir. When the amount of grain in the reservoir is substantially larger, the tsunami wave speed dominates the submarine debris wave. Another important aspect is the increased basal drag (basal friction for the solid phase) with the increased solid load in the dam. This is modeled by the term associated with the factor $\tan\delta$. This virtually does not directly effect the motion of the tsunami but increases the basal friction for the solid phase. Thus, increasing the amount of the solid in the reservoir means increasing the basal friction for the solid phase. Changing the solid volume fraction also means changing the solid pressure gradient. The simulation indicates that the increasing amount of the grains in the reservoir may imply the relatively smaller solid pressure gradient in the downstream direction. This effectively slows down the motion. This effect is associated with the pressure gradient factor β_s. Also, there are other nonlinear and implicit interactions between the solid and the fluid with changing amount of the solid in the reservoir as there are strong nonlinear interactions between the solid and the fluid in the real two-phase mass flow model. This includes the changing virtual mass force (C) and the non-Newtonian viscous stress (N_{R_A}) as both of them are changing with changing amount of α_s (the solid concentration) in the reservoir. Simulation results may be altered by changing the physical parameters. However, here, we are mainly interested in investigating the competition between the submarine debris wave and surface tsunami (with simple simulations). This is achieved by systematically changing the solid concentration in the reservoir.

The main aspect of this paper was to present and highlight some basic mechanisms of two-phase debris flow, its impact to and interaction with an initially quiet fluid reservoir, submarine debris flow, and complex wave interactions including submarine debris wave and surface tsunami. Another aspect was to investigate the model performance through some numerical simulations. However, the simulation results have yet to be compared and validated with laboratory and/or field data, which is not within the scope of the present work. Furthermore, here, only the geometrically two-dimensional (velocity-wise one-dimensional) two-phase submarine debris flows and associated tsunami have been presented. These results present only a possible basic scenario, which however, may be much more complicated when dealing with the complex flows in a real three-dimensional natural setting with lateral spreading, diffusion and accumulation during the deposition processes, and their applications with GIS or DTM [9,29]. These results can also be extended to more complete and full-dimensional simulations without depth-averaging [5,6]. One of the very interesting future works would be to perform simple small scale laboratory experiments in which the solid concentration in the reservoir can be changed systematically in order to investigate the dynamics of two-phase submarine debris flow and to utilize these data to validate the model and the simulation results.

6 Summary

The simultaneous dynamic simulation of the two-phase subaerial debris flow, the resulting tsunami generation and propagation upon debris impact at the reservoir, the subsequent submarine debris flow, and the entire analysis of all three types of waves and their complex interactions were studied by applying a generalized two-phase debris flow model (Pudasaini, 2012) [43], and are simulated together with a high-resolution shock-capturing scheme. We analyze in detail on how the subaerial debris mass penetrates the fluid reservoir and finally how it moves and deposits on the bottom of the reservoir basin. Here, we show that the amount of solid grains in the reservoir plays a significant role in controlling the overall dynamics of the submarine debris flow and the tsunami wave. It is observed that for a small amount of solid volume fraction in the reservoir, the submarine debris flow moves substantially faster than the tsunami generated by a two-phase debris flow itself.

As the amount of the solid in the reservoir increases, the submarine debris speed slows down and above some higher value of the solid volume fraction in the reservoir the tsunami wave speed clearly exceeds the submarine debris speed. These results may be observable in nature. This is a novel and important result that can be used to generate early warning signals in coastal regions, and also to prevent possible catastrophic dam collapses, e.g., the hydro-power dam prone to be hit by landslides. The competition between the submarine debris wave speed and the tsunami speed is attributed to the friction generating mechanisms such as the drag, basal friction, the force associated with the pressure gradient of the solid phase, virtual mass, and non-Newtonian viscous stresses. For small solid concentration gradients in the reservoir, as the submarine debris flow impinges the distal vertical wall of the dam, a debris shock wave is generated and propagates upstream, where it is eventually diffused. Our innovative and unified approach allows for the adequate modeling of debris-induced tsunami and submarine sediment transport, with applications in sedimentology, submarine geodynamics, the integrity of hydroelectric power plants, and hazard mitigation.

Acknowledgments We would like to thank very much Martin Mergili and two anonymous reviewers for their constructive reviews that substantially improved the quality of this paper.

References

1. Abadie, S., Morichon, D., Grilli, S., Glockner, S.: Numerical simulation of waves generated by landslides using a multiple-fluid Navier–Stokes model. Coast. Eng. **57**(9), 779–794 (2010)
2. Abele, G.: Kinematik und Morphologie spät- und postglazialer Bergstürze in den Alpen. Z. Geomorph. N.F. Suppl. Bd. **14**, 138–149 (1972)
3. Antobreh, A.A., Krastel, S.: Mauritania Slide Complex: morphology, seismic characterisation and processes of formation. Int. J. Earth Sci. (Geol. Rundsch.) **96**, 451–472 (2007). doi:10.1007/s00531-006-0112-8
4. Cecioni, C., Bellotti, G.: Inclusion of landslide tsunamis generation into a depth integrated wave model. Nat. Hazards Earth Syst. Sci. **10**, 2259–2268 (2010)
5. Domnik, B., Pudasaini, S.P.: Full two-dimensional rapid chute flows of simple viscoplastic granular materials with a pressure-dependent dynamic slip-velocity and their numerical simulations. J. Non-Newtonian Fluid Mech. **173–174**, 72–86 (2012)
6. Domnik, B., Pudasaini, S.P., Katzenbach, R., Miller, S.A.: Coupling of full two-dimensional and depth-averaged models for granular flows. J. Non-Newtonian Fluid Mech. **201**, 56–68 (2013)
7. Fernandez-Nieto, E.D., Bouchut, F., Bresch, D., Castro Diaz, M.J., Mangeney, A.: A new Savage–Hutter type model for submarine avalanches and generated tsunami. J. Comput. Phys. **227**, 7720–7754 (2008)
8. Fine, I.V., Rabinovich, A.B., Bornhold, B.D., Thomson, R.E., Kulikov, E.A.: The Grand banks landslide generated tsunami of November 18, 1929: preliminary analysis and numerical modeling. Mar. Geol. **215**, 45–57 (2005)
9. Fischer, J.T., Kowalski, J., Pudasaini, S.P.: Topographic curvature effects in applied avalanche modeling. Cold Reg. Sci. Tech. **74-75**, 21–30 (2012)
10. Foerster, A., Ellis, R.G., Henrich, R., Krastel, S., Kopf, A.J.: Geotechnical characterization and strain analyses of sediment in the Mauritania Slide Complex, NW-Africa. Mar. Pet. Geol. **27**, 1175–1189 (2010)
11. Geersen, J., Voelker, D., Behrmann, J.H., Reichert, C., Krastel, S.: Pleistocene giant slope failures offshore Arauco Peninsula, Southern Chile. J. Geol. Soc. Lond. **168**, 1–12 (2011). doi:10.1144/0016-76492011-027
12. George, D.L., Iverson, R.M.: A two-phase debris-flow model that includes coupled evolution of volume fractions, granular dilatancy, and pore-fluid pressure. Italy J. Eng. Geol. Environ. (2011). doi:10.4408/IJEGE.2011-03.B-047
13. Georgiopoulou, A., Masson, D.G., Wynn, R.B., Krastel, S.: Sahara slide: age, initiation, and processes of a giant submarine slide. Geochem. Geophys. Geosyst. **11**, Q07014 (2010). doi:10.1029/2010GC003066
14. Haflidason, H. et al.: A weak layer feature on the Northern Storegga Slide escarpment. In: Mienert, J., Weaver, P. (eds.) European Margin Sediment Dynamics, Side-Scan Sonar and Seismic Images, pp. 55–62. Springer, Berlin (2003)
15. Harbitz, C.B., Lovholt, F., Pedersen, G., Masson, D.G.: Mechanisms of tsunami generation by submarine landslides: a short review. Norw. J. Geol. **86**(3), 255–264 (2006)
16. Haugen, K.B., Lovholt, F., Harbitz, C.B.: Fundamental mechanisms for tsunami generation by submarine mass flows in idealised geometries. Mar. Pet. Geol. **22**(1–2), 209–217 (2005)
17. Henkel, S. et al.: An interdisciplinary investigation of a recent submarine mass transport deposit at the continental margin off Uruguay. Geochem. Geophys. Geosyst. **12**, Q08009 (2011). doi:10.1029/2011GC003669
18. Henrich, R., Hanebuth, T., Krastel, S., Neubert, N., Wynn, R.B.: Architecture and sediment dynamics of the Mauritania Slide Complex. Marine Petrol. Geol. **25**, 17–33 (2008)
19. Iverson, R.M., Denlinger, R.P.: Flow of variably fluidized granular masses across three-dimensional terrain: 1. Coulomb mixture theory. J. Geophys. Res. **106**(B1), 537–552 (2001)
20. Jerz, H., Poschinger, A.V.: Neuere Ergebnisse zum Bergsturz Eibsee-Grainau. Geologica Bavarica **99**, 383–398 (1995)
21. Kowalski, J., McElwaine, J.N.: Shallow two-component gravity-driven flows with vertical variation. J. Fluid Mech. **714**, 434–462 (2013)
22. Krastel, S., Scminke, H.U., Jacobs, C.L., Rihm, R., Le Bas, T.P., Alibes, B.: Submarine landslides around the Canary Islands. J. Geophys. Res. **106**, 3977–3997 (2001)
23. Krastel, S.: Cruise Participants: Report and Preliminary Results of Meteor Cruise M 65/2, Dakar-Las Palmas 04.07.–26.07.2005, Berichte, Fachbereich Geowissenschaften, Universitaet Bremen, p. 249 (2006)

24. Liu, P.L.F., Wu, T.R., Raichlen, F., Synolakis, C.E., Borrero, J.C.: Runup and rundown generated by three-dimensional sliding masses. J. Fluid Mech. **536**(1), 107–144 (2005)
25. Masson, D.G., Harbitz, C.B., Wynn, R.B., Pedersen, G., Lovholt, F.: Submarine landslides: processes, triggers and hazard prediction. Phil. Trans. R. Soc. A 364, 2009–2039 (2006)
26. Martinez, M.L. et al.: The coasts of our world: ecological, economic and social importance. Ecol. Econ. **63**, 254–272 (2007)
27. Maxey, R.M., Riley, J.J.: Equation of motion for a small sphere in a non-uniform flow. Phys. Fluids **26**, 883–889 (1993)
28. McAdoo, B.G., Watts, P.: Tsunami hazard from submarine landslides on the Oregon continental slope. Marine Geol. **203**, 235–245 (2004)
29. Mergili, M., Schratz, K., Ostermann, A., Fellin, W.: Physically-based modelling of granular flows with Open Source GIS. Nat. Hazards Earth Syst. Sci. **12**, 187–200 (2012)
30. Miller Don, J.: Giant Waves in Lituya Bay, Alaska. Geological Survey Professional Paper 354-C, U.S. Government Printing Office, Washington (1960)
31. Miller, L.: The rock slide in the Vajont Valley. Rock Mech. Eng. GeoZ. **2**(3–4), 148–212 (1964)
32. Mohammed, F., Fritz, H.M.: Experiments on tsunamis generated by 3D granular landslides. In: Mosher, D.C. et al. (eds.) Submarine Mass Movements and Their Consequences, 4th International Symposium. Advances in Natural and Technological Hazards Research, vol. 28, pp. 705–718. Springer, New York (2010)
33. Montagna, F., Bellotti, G., Di Risio, M.: 3D numerical modeling of landslide-generated tsunamis around a conical island. Nat. Hazards **58**(1), 591–608 (2011)
34. Nessyahu, H., Tadmor, E.: Non-oscillatory central differencing for hyperbolic conservation laws. J. Comput. Phys. **87**, 408–463 (1990)
35. Pierau, R., Hanebuth, T.J.J., Krastel, S., Henrich, R.: Late Quaternary climatic events and sea-level changes recorded by turbidite activity, Dakar Canyon, NW Africa. Quat. Res. **73**, 385–392 (2010)
36. Pierau, R., Henrich, R., Preiss-Daimler, I., Krastel, S., Geersen, J.: Sediment transport and turbidite architecture in the submarine Dakar Canyon off Senegal, NW-Africa. J. Afr. Earth Sci. **60**, 196–208 (2011)
37. Pitman, E.B., Le, L.: A two-fluid model for avalanche and debris flows. Philos. Trans. R. Soc. **A363**, 1573–1602 (2005)
38. Pudasaini, S.P., Hutter, K.: Rapid shear flows of dry granular masses down curved and twisted channels. J. Fluid Mech. **495**, 193–208 (2003)
39. Pudasaini, S.P., Wang, Y., Hutter, K.: Modelling debris flows down general channels. Nat. Hazards Earth Syst. Sci. **5**, 799–819 (2005)
40. Pudasaini, S.P., Hutter, K.: Avalanche Dynamics: Dynamics of Rapid Flows of Dense Granular Avalanches. pp. 602 Springer, New York (2007)
41. Pudasaini, S.P., Kröner, C.: Shock waves in rapid flows of dense granular materials: theoretical predictions and experimental results. Phys. Rev. E **78**, 041308 (2008). doi:10.1103/PhysRevE.78.041308
42. Pudasaini, S.P.: Some exact solutions for debris and avalanche flows. Phys. Fluids **23**(4), 043301 (2011)
43. Pudasaini, S.P.: A general two-phase debris flow model. J. Geophys. Res. **117**, F03010. (2012). doi:10.1029/2011JF002186
44. Pudasaini, S.P., Miller, S.A.: Buoyancy induced mobility in two-phase debris flow. Am. Inst. Phys. Proc. **1479**, 149–152 (2012a). doi:10.1063/1.4756084
45. Pudasaini, S.P., Miller, S.A.: A real two-phase submarine debris flow and tsunami. Am. Inst. Phys. Proc. **1479**, 197–200 (2012b). doi:10.1063/1.4756096
46. Pudasaini, S.P., Miller, S.A.: The hypermobility of huge landslides and avalanches. Eng. Geol. (2013). doi:10.1016/j.enggeo.2013.01.012
47. Rivero, M., Magnaudet, J., Fabre, J.: Quelques resultants nouveaux concernat les forces exercees sur une inclusion spherique par un ecoulement accelere. C. R. Acad. Sci. Ser. II **312**, 1499–1506 (1991)
48. Savage, S.B., Hutter, K.: The motion of a finite mass of granular material down a rough incline. J. Fluid Mech. **199**, 177–215 (1989)
49. Takahashi, T.: Debris Flow: Mechanics, Prediction and Countermeasures. Taylor & Francis, London (2007)
50. Tai, Y.-C., Noelle, S., Gray, J.M.N.T., Hutter, K.: Shockcapturing and front-tracking methods for granular avalanches. J. Comput. Phys. **175**, 269–301 (2002)
51. Tinti, S., Armigliato, A., Manucci, A., Pagnoni, G., Zaniboni, F., Yalciner, A.C., Altinok, Y.: The generating mechanisms of the August 17 1999 Izmit bay (Turkey) tsunami: Regional (tectonic) and local (mass instabilities) causes. Marine Geol. **225**, 311–330 (2006)
52. Tinti, S., Manucci, A., Pagnoni, G., Armigliato, A., Zaniboni, F.: The 30 December 2002 landslide-induced tsunamis in Stromboli: sequence of the events reconstructed from the eyewitness accounts. Nat. Hazards Earth Syst. Sci. **5**, 763–775 (2005)
53. Watts, P., Grilli, S.T., Tappin, D.R., Fryer, G.J.: Tsunami generation by submarine mass failure. II: predictive equations and case studies. J. Waterw. Port Coast. Ocean Eng. **131**(6), 298–310 (2005)
54. Weiss, R., Fritz, H.M., Wuennemann, K.: Hybrid modeling of the mega-tsunami runup in Lituya Bay after half a century. Geophys. Res. Lett. **36**, L09602 (2009). doi:10.1029/2009GL037814